SCIENTIFIC REPORTS

OPEN

A 200-year annually laminated stalagmite record of precipitation seasonality in southeastern China and its linkages to ENSO and PDO

Haiwei Zhang [1,2,3], Hai Cheng[1,4], Christoph Spötl[3], Yanjun Cai[1,2], Ashish Sinha[5], Liangcheng Tan [1,2], Liang Yi[6], Hong Yan[2], Gayatri Kathayat[1], Youfeng Ning[1], Xianglei Li[1], Fan Zhang[1], Jingyao Zhao[1] & R. Lawrence Edwards[4]

In southeastern China (SEC), the precipitation amount produced by the East Asian summer monsoon (EASM) is almost equivalent to that during the non-summer monsoon (NSM) period, both of them significantly affecting agriculture and socioeconomy. Here, we present a seasonally-resolved stalagmite $\delta^{18}O$ record ($\delta^{18}O_s$) for the interval 1810–2009 AD from E'mei cave, Jiangxi Province, SEC. The comparison between $\delta^{18}O_s$ and instrumental data indicates that the $\delta^{18}O_s$ variability is primarily controlled by the precipitation seasonality (i.e., the ratio of EASM/NSM precipitation) modulated by the El Niño/Southern Oscillation (ENSO) on interannual to interdecadal timescales. Higher (lower) $\delta^{18}O_s$ values thereby correspond to lower (higher) EASM/NSM ratios associated with El Niño (La Niña) events. Significant correlations with ENSO and the Pacific Decadal Oscillation (PDO) indicate that the precipitation seasonality in SEC is remarkably influenced by ocean-atmosphere interactions, with lower (higher) EASM/NSM ratios during warm (cold) phases of ENSO/PDO. The progressive increase in $\delta^{18}O_s$ since 2005 AD may reflect a strengthening of the central Pacific El Niño under continued anthropogenic global warming. The relationship between seasonal precipitation and $\delta^{18}O_s$ with ENSO/PDO requires further studies.

Southeastern China (SEC), which is one of the most densely populated areas in East Asia, is significantly influenced by summer floods and droughts associated with the East Asian summer monsoon (EASM)[1]. For example, in 1998, more than 1,000 people were killed and more than 200 million people were affected by the floods in the middle and lower reaches of Yangtze River Valley (YRV), and the direct socioeconomic losses amounted to about £10,000 million[2]. In addition, the spring rainy period in SEC[3], associated with low temperatures, overcast and rain, is also a severe threat to agriculture (e.g., cotton plants) and transportation[4,5]. Studies indicate that the rainy season in SEC includes the EASM and spring rainfall and both of them show high variability[4,6]. Frequent flood and drought events resulting from this seasonally variable precipitation seriously impact agriculture and socioeconomy in this region. Therefore, it is essential to study the variability in precipitation seasonality and assess its influencing factors.

Observations and simulations demonstrate that ENSO and PDO have a major impact on the interannual-interdecadal variability in precipitation over SEC[7–17]. Some investigated the combined effects of PDO[7–9] and ENSO[10–15] on EASM, spring or East Asian winter monsoon (EAWM) precipitation over Eastern China, respectively. Others examined the modulation of the relationship between ENSO and EASM[11,16], spring[6] or EAWM[17] precipitation by the PDO. However, the relationship between precipitation variability and ENSO/PDO on interannual to interdecadal timescales remains poorly understood, partly due to the limited availability

[1]Institute of Global Environmental Change, Xi'an Jiaotong University, Xi'an, 710054, China. [2]Institute of Earth Environment, Chinese Academy of Sciences, State Key Laboratory of Loess and Quaternary Geology, Xi'an, 710061, China. [3]Institute of Geology, University of Innsbruck, Innsbruck, 6020, Austria. [4]Department of Earth Science, University of Minnesota, Minneapolis, Minnesota, 55455, USA. [5]Department of Earth Science, California State University Dominguez Hills, Carson, California, 90747, USA. [6]State Key Laboratory of Marine Geology, Tongji University, Shanghai, 200092, China. Correspondence and requests for materials should be addressed to H.Z. (email: zhanghaiwei@xjtu.edu.cn)
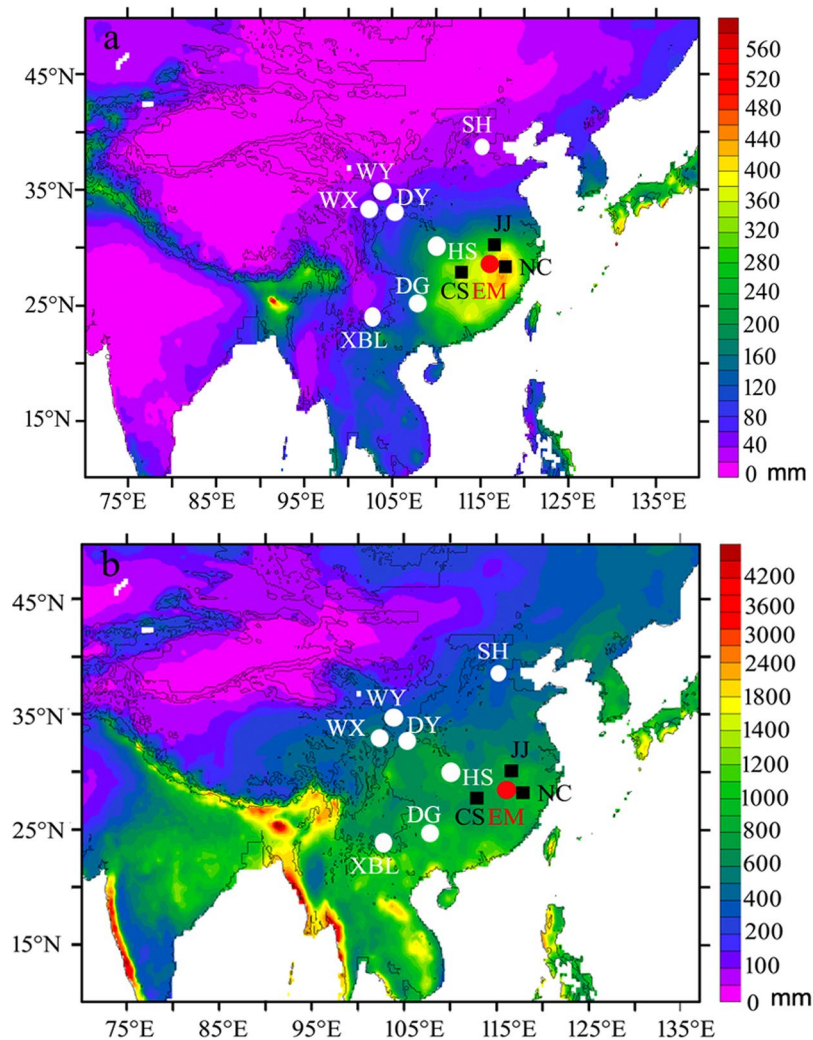
Figure 1. Overview map showing the spatial distribution of seasonal precipitation amount in China and other locations mentioned in this study. The backgrounds in (**a**) and (**b**) are the distribution of mean SPR (March–April) and EASM (May–September) precipitation amount in China from 1951 to 2007, respectively. The red dot denotes the location of E'mei Cave (this study), and the white dots indicate the Shihua[28] (SH), Wuya[22] (WY), Wanxiang[27] (WX), Dayu[47] (DY), Heshang[61] (HS), Dongge[38] (DG) and Xiaobailong[62] (XBL) cave sites in the monsoon region of China. The black squares mark the Jiujiang (JJ), Nanchang (NC) and Changsha (CS) meteorological stations. The map was exported based on the precipitation data source (1951–2007) from APHRODITE (Asian Precipitation-Highly-Resolved Observational Data Integration Towards Evaluation of Water Resources, APHRO_MA_V1101R2 product, (21). Website: http://www.chikyu.ac.jp/precip/)[63].

of instrumental datasets. In addition, most researchers focused on the variations of EASM or EAWM in the Asian monsoon region, and only few studies examined the variability in precipitation seasonality[18]. Long-term paleoclimatic reconstructions are needed to explore the variability of precipitation in SEC and its seasonality.

Some $\delta^{18}O$ records of tree-ring cellulose in SEC were recently published[18–20], but they mainly constrain precipitation and relative humidity during the rainy season. High-precision and high-resolution $\delta^{18}O$ records of stalagmite ($\delta^{18}O_s$), calibrated against instrumental data, can be used to reconstruct the variability of ENSO/PDO in the past. In this study, we present a first seasonally-resolved $\delta^{18}O_s$ record for the period 1810–2009 AD based on an annually laminated stalagmite from E'mei cave, Jiangxi Province, SEC. This record allows us to explore the variability in the precipitation seasonality modulated by ENSO and PDO on interannual to interdecadal timescales.

Cave Location, Sample and Climate

E'mei Cave (115°29′44″E, 29°33′18″N, 53 m a.s.l.) is located in the north of Jiangxi Province, SEC (Fig. 1). The hostrock is a Middle Ordovician limestone. An actively growing calcitic stalagmite (EM1) of 60 mm in height (Supplementary Fig. S1) was collected ~150 m behind the entrance of the cave in December 2009. The regional climate is subtropical humid and the rainy season includes spring (March to May) and summer (June to August) (Supplementary Fig. S2). Instrumental data from the Nanchang and Jiujiang meteorological stations (1951–2010 AD) show that mean annual precipitation is 1514 mm and the annual temperature is 17.3 °C. The EASM
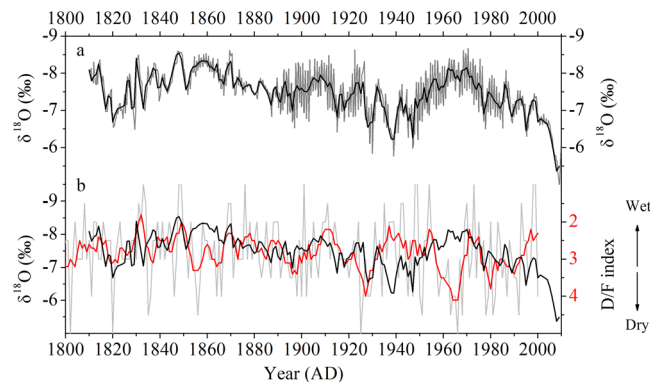
Figure 2. (**a**) The original δ18O (grey line) record and the averaged annually resolved δ18O (black line) record of stalagmite EM1. (**b**) Comparison between annually resolved EM1 δ18O (black line) and D/F index (hoar line) records. The red line is the 5-year smoothing average curve of D/F index. The annual D/F index, based on the abundance of drought and flood events during spring, summer and autumn as recorded in historical documents[39] reflects the local precipitation variation.

(May to September) precipitation with lower δ18O values accounts for 54% of the annual precipitation and the non-summer monsoon (NSM) (October to next April) precipitation with higher δ18O values accounts for 46% (Supplementary Fig. S2). The amount-weighted mean annual precipitation δ18O ($\delta^{18}O_w$) value is controlled by both EASM and NSM precipitation. Data from the nearest GNIP station (Changsha station, about 100 km west of E'mei Cave) during 1988–1992 indicate lower $\delta^{18}O_w$ values, more June-September precipitation and less March-April precipitation during La Niña years as compared to El Niño years (Supplementary Fig. S3). Therefore, the variation in $\delta^{18}O_w$ during 1988–1992 is probably influenced by the ratio of EASM/NSM precipitation but not by the amount of annual precipitation which lacks a significant variation (Supplementary Fig. S3).

Results

Chronology. Elevated detrital 232Th levels of 2–4×10^3 ppt resulted in large dating uncertainties of 172–438 years for 230Th dates (Supplementary Table S1 and Fig. S4) and hinder precise age models. Although the dating errors are large, the 230Th dates still indicate that stalagmite EM1 grew during about last 200 years, which is consistent with the 200 ± 3 well-developed laminae within errors (see next paragraph). The 230Th dates at 6 and 18.5 mm from the top are 1997 ± 267 and 1932 ± 158 AD, respectively, and the inferred age of the top of EM1 is 2028 ± 267 AD. This is consistent with the observation of active dripping when this stalagmite was collected in December 2009. The top age of EM1 was therefore assumed to be late 2009 AD.

The cross-section of EM1 shows continuous, well-developed laminae consisting of alternating dense, translucent sub-layers (TDSL) and white, porous sub-layers (WPSL)[21,22] (Supplementary Fig. S1). The visible WPSL are opaque under the transmitted-light microscope, but brightly luminescent under mercury light source UV reflected light and in the confocal laser fluorescent microscope (CLFM) (Supplementary Fig. S1), which is consistent with observations from other caves[21,23]. As suggested by previous studies, the fluorescent sub-layer forms from organic-rich dripwater during the wet season, while dripwater depleted in organics during the dry season results in the non-fluorescent sub-layer[23]. We identified a total of 159 $\delta^{18}O_s$ cycles between 0 and 45.6 mm from the top of EM1, consistent with 159 bright-dark couplets, confirming the annual nature of these highly regular laminae (Supplementary Fig. S5b and c). 200 ± 3 bright-dark couplets were counted using CLFM between 0 and 53.6 mm from the top of EM1. The number of annual laminae and $\delta^{18}O_s$ cycles was used to establish an age model for EM1 (Supplementary Figs S4 and S5), considering that EM1 grew continuously from 1810 to 2009 AD, which is consistent with the 230Th dates within errors.

In order to constrain the chronology of EM1, we also compared the δ18O and δ13C records of EM1 with stalagmite YQ15-1, which was obtained from Yongquan Cave, 50 km northeast of E'mei Cave. The dating errors of YQ15-1 (12–15 years, Supplementary Fig. S5a) are much smaller than those of EM1. The δ18O and δ13C records of YQ15-1 and EM-1 replicate well (Supplementary Fig. S5a), further confirming the EM1 chronology.

δ18Os record. There are clear annual $\delta^{18}O_s$ cycles between 0 and 45.6 mm from the top of EM1, while these cycles are less clear between 45.6 and 53.6 mm because of a slower growth rate (Supplementary Fig. S4). We therefore interpolated this interval by using the corresponding relationship between the micromilling track of stable isotope analyses and layer counting (Supplementary Fig. S1b). Together with the 159 annual $\delta^{18}O_s$ cycles between 0 and 45.6 mm, δ18O and δ13C records of EM1 were established for the period 1810–2009 AD (Fig. 2a). The good replication of the stable isotope records between EM1 and YQ15-1 indicates that EM1 was deposited close to isotope equilibrium conditions[24,25], although "Hendy tests"[26] yielded a significant correlation (r = 0.31, p < 0.01, n = 780) between δ18O and δ13C values along the growth axis. The co-variation of δ18O and δ13C can also result from the climatic and environmental change[24]. The inverse relationship between δ18O and δ13C values on seasonal timescales (Supplementary Fig. S5b) further indicates that kinetic isotope fractionation has a negligible effect only and the $\delta^{18}O_s$ signal recorded in EM1 is primarily of climatic origin.
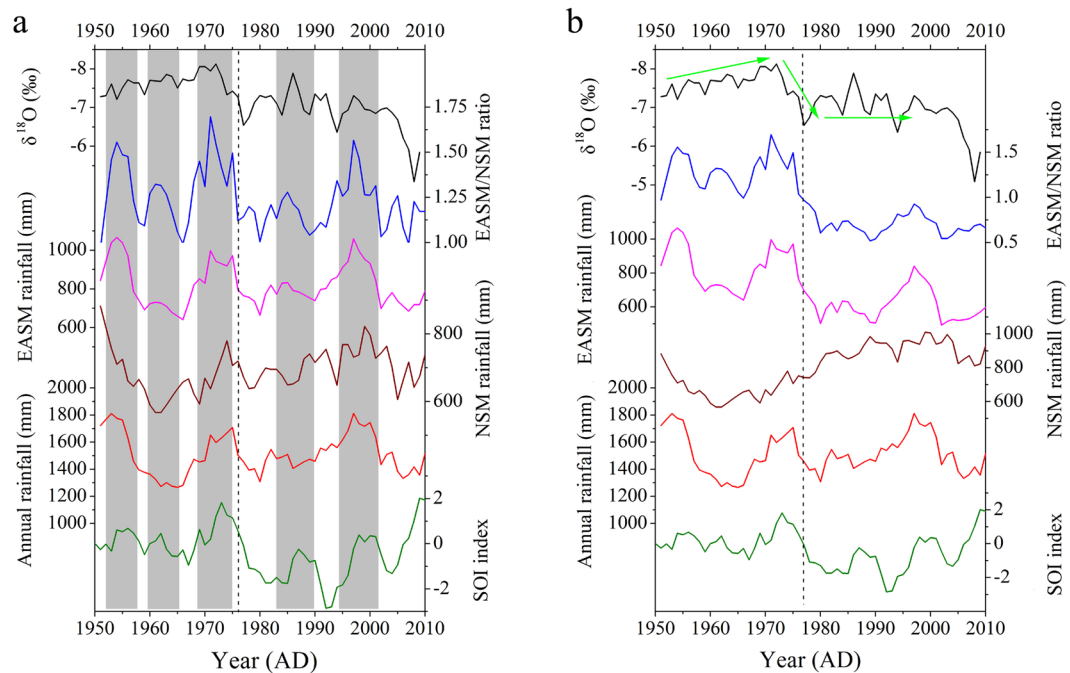
Figure 3. Comparison between EM1 $\delta^{18}O$ (black line), SOI index (green line) and instrumental precipitation (EASM (pink), NSM (brown) and annual (red) precipitation and EASM/NSM ratio (blue)) in the study area during 1951–2010 AD. In (**a**) the EASM rainfall is represented by May-September precipitation and NSM rainfall is represented by October-April precipitation during 1951–2010 AD; In (**b**) the May-September and October-April precipitation is used to represent EASM and NSM precipitation in 1951–1976 AD, respectively. The June-September and October-May precipitation is used to represent EASM and NSM precipitation for 1977–2010 AD, respectively. EASM and NSM precipitation was adjusted after the shifts of PDO/ENSO in 1976–1977 AD (dashed line), because the EASM starts late (early) and tends to be weaker (stronger) during El Niño (La Niña) years[41].

Discussion

Significance of $\delta^{18}O_s$ proxy. Although $\delta^{18}O_s$ variability in the monsoon region of China on orbital to millennial timescales generally reflects the variation of EASM intensity, its significance on short timescales remains to be understood. Previous studies demonstrated that the $\delta^{18}O_s$ variability in the marginal zone of the EASM reflects the variation of monsoon intensity or precipitation amount[22,27,28]. In SEC, however, this relationship is more complex, because of the various factors influencing precipitation $\delta^{18}O$ ($\delta^{18}O_p$), e.g., precipitation amount, moisture sources, moisture pathways and rainfall seasonality. Dayem *et al.*[29] suggested that several processes associated with precipitation seasonality might jointly influence the fluctuation of Chinese $\delta^{18}O_s$[29]. Based on the analyses of modern precipitation $\delta^{18}O$ data[30], Tan[31] suggested that $\delta^{18}O_s$ in the monsoon region of China records the moisture source changes related to ENSO circulation but not the monsoon intensity or precipitation amount. The higher $\delta^{18}O_s$ values reflect more moisture originating from the adjacent Pacific Ocean relative to the remote Indian Ocean during El Niño phases, and vice versa[31]. However, some studies suggested that EASM precipitation is primarily derived from the Indian Ocean, while the moisture from the West Pacific Ocean is a minor contributor to monsoonal rainfall only[32,33], and the $\delta^{18}O_p$ variability is caused by both precipitation amount and moisture transport history[32]. Cheng *et al.*[34] and Yang *et al.*[35] suggested that $\delta^{18}O_s$ is primarily controlled by large-scale monsoon intensity and upstream precipitation. As introduced above, $\delta^{18}O_w$ in the study area is influenced by both the EASM and the NSM associated with ENSO circulation (Supplementary Fig. S2). Thus, the EM1 $\delta^{18}O_s$ record was compared to the instrumental seasonal precipitation and the Southern Oscillation Index (SOI) in order to explore its significance on interannual to interdecadal timescales.

On an interannual timescale, the comparison between $\delta^{18}O_s$ and the SOI shows a significantly negative correlation (Fig. 3a, r = −0.50, p < 0.01 using a 5-year moving average for 1951–2004 AD), with higher (lower) $\delta^{18}O_s$ during El Niño (La Niña) events. This is consistent with previous studies based on instrumental data[30,33,35] and $\delta^{18}O$ records of tree-ring cellulose[18–20,36] and stalagmites[37,38] in SEC. $\delta^{18}O_s$ is significantly and negatively correlated with the ratio of EASM/NSM precipitation (r = −0.32, p < 0.05) using a 5-year moving average for 1951–2009 AD (Fig. 3a). There is no significant correlation between $\delta^{18}O_s$ and the EASM, NSM and annual precipitation, although a good coherent variation can be observed (grey bars in Fig. 3a). We also compared the interannual variation between EM1 $\delta^{18}O_s$ and the local Drought/Flood (D/F) index for 1810–2000 AD. The annual D/F index, based on drought or flood events in spring, summer and autumn recorded in historical documentaries[39], can reflect local precipitation variations in May-September, with a decreased (increased) D/F index representing more (less) precipitation. The good coherence indicates that lower (higher) $\delta^{18}O_s$ values are associated with increased (decreased) EASM precipitation in the study area (Fig. 2b).

PDO and ENSO are strongly correlated on decadal timescales[11], with warm PDO phases (positive PDO index) corresponding to warm ENSO phases (El Niño phases, negative SOI index). On an interdecadal timescale, previous studies demonstrated that the PDO/ENSO circulation shifted from a cold phase during 1951–1976 AD to a warm phase during 1977–2000 AD[7,11]. During the cold phase of PDO/ENSO, EM1 $\delta^{18}O_s$ values are generally lower than during the subsequent warm phase (green arrows in Fig. 3a), whereas precipitation amount does not show a significantly systematic shift (Fig. 3a). Actually, studies demonstrated that the intensity and duration of the EASM have a strong variability on interdecadal timescales[40]. The EASM starts late (early) and tends to be weaker (stronger) during El Niño (La Niña) years[41], and the onset varies from late April to early June[40,41]. Thus, May-September precipitation cannot be always used to represent the EASM precipitation, especially in SEC characterized by a strong precipitation seasonality. This is also supported by instrumental $\delta^{18}O_p$ data from the Changsha GNIP station (Supplementary Fig. S6). They show that the $\delta^{18}O_p$ values in May during La Niña years (1988–1989 AD) are lower than those during El Niño years (1991–1992 AD), indicating that the EASM starts early (late) during La Niña events (El Niño events). Therefore, EASM precipitation during 1951–1976 AD likely represented May-September precipitation, while it shifted to June-September precipitation during 1977–2010 AD; the NSM precipitation should be adjusted accordingly. Hence, less EASM and more NSM precipitation results in higher $\delta^{18}O_s$ values during long-term El Niño phases (Fig. 3b) and vice versa.

Similarly, the poor correlation between $\delta^{18}O_s$ and the D/F index during 1930–1970 AD on an interdecadal timescale (Fig. 2b) might be caused by the variation of precipitation seasonality associated with shifts in oceanic-atmospheric circulation. We calculated the correlation coefficients between $\delta^{18}O_s$ and the adjusted EASM and NSM precipitation as well as EASM/NSM ratios using a 5-year moving average for 1951–2009 AD. The data show that $\delta^{18}O_s$ is significantly negatively correlated with the ratio of EASM/NSM precipitation (r = −0.67, p < 0.01) and the EASM precipitation (r = −0.54, p < 0.01), and is significantly positively correlated with the NSM precipitation (r = 0.58, p < 0.01), suggesting that higher (lower) $\delta^{18}O_s$ values are associated with lower (higher) EASM/NSM ratios during El Niño (La Niña) phases on interannual to interdecadal timescales.

Considering the strong precipitation seasonality (including precipitation amount and moisture sources/pathways) in the study area, we suggest that the EASM/NSM ratio better explains the $\delta^{18}O_s$ variation on interannual-interdecadal timescales. Studies demonstrated that EASM precipitation is mainly sourced from the remote Indian Ocean while NSM precipitation primarily originates from the adjacent Pacific Ocean[32,33]. Thus, the EASM/NSM ratio may also represent the ratio of moisture sources/pathways during the EASM season to that of the NSM season, partly similar to the "circulation effect" proposed by Tan[31]. He suggested that the $\delta^{18}O_p$ and $\delta^{18}O_s$ values are affected by the variation of moisture source in the summer monsoon season. We also emphasize the influence of NSM precipitation, which accounts for 45~65% of the annual precipitation in the study area. As a consequence, we suggest that the variation in precipitation seasonality (e.g., EASM/NSM ratio) modulated by ENSO plays a key factor in controlling the $\delta^{18}O_s$ variability in the study area on interannual to interdecadal timescales, with higher (lower) $\delta^{18}O_s$ values reflecting lower (higher) EASM/NSM ratios associated with El Niño (La Niña) phases.

Links between $\delta^{18}O_s$, precipitation seasonality and ocean-atmosphere interaction.

The comparison between EM1 $\delta^{18}O_s$ and the PDO index shows a significantly positive correlation (Fig. 4, r = 0.27, p < 0.01, applying a 5-year average for 1854–2004 AD), with higher (lower) $\delta^{18}O_s$ values corresponding to warm (cold) PDO phases. A positive correlation between the PDO and the $\delta^{18}O$ record was also observed in other records from speleothem[22,28,42–45] and tree-ring cellulose[36,46] in the monsoon region of China. The EM1 $\delta^{18}O_s$ is significantly negatively correlated with the SOI index (Fig. 4, r = −0.32, p < 0.01, applying a 5-year average for 1866–2004 AD), with higher (lower) $\delta^{18}O_s$ values corresponding to El Niño (La Niña) phases. This is consistent with the relationship between $\delta^{18}O_s$ and the SOI index during 1951–2004 AD (Fig. 3) and other studies based on simulations and reconstructions discussed above. Studies demonstrated that the effect of ENSO or PDO on EASM precipitation in SEC is significant by modulating the position and intensity of the western Pacific subtropical high (WPSH), which changes under different phases of PDO/ENSO[1,8,40]. WPSH intensities enhance (weaken) and the western ridge point moves westward (eastward) during El Niño (La Niña) phases[41]. Based on a comparison between instrumental $\delta^{18}O_p$ data and the WPSH strength (WPSH$_s$) index, Tan[30] showed that increased $\delta^{18}O_p$ values in SEC are associated with a strengthening and westward expansion of the WPSH during the summer following an El Niño event. The comparison between the WPSH$_s$ index and $\delta^{18}O_s$ yielded a significantly positive correlation (Fig. 4, r = 0.61, p < 0.01, after applying a 5-year moving average for 1900–2009 AD), with higher (lower) $\delta^{18}O_s$ corresponding to a strengthened (weakened) WPSH. Positive correlations between WPSH intensity and $\delta^{18}O$ records were also reported from the monsoon region of China based on stalagmites and tree-ring cellulose[19,22,31]. As a consequence, the comparison between $\delta^{18}O_s$, WPSH$_s$, ENSO and PDO reveals that higher (lower) $\delta^{18}O_s$ values represent a strengthened (weakened) WPSH associated with warm (cold) phases of PDO/ENSO on interannual to interdecadal timescales. This indicates a lower (higher) EASM/NSM ratio in the study area during a warm (cold) phase of PDO/ENSO. The significant 55–66 year cycle observed in the EM1 $\delta^{18}O_s$ time series is generally consistent with the 50–70 year cycle seen in the PDO records[22]. The significant 2.4, 3.2 and 5.7-year cycles in the EM1 $\delta^{18}O_s$ time series are consistent with 2–7 year cycles in ENSO records, further supporting the important influence of PDO and ENSO on precipitation variation (Supplementary Fig. S7).

A comparison of available high-resolution $\delta^{18}O_s$ records from annually laminated or high-precisely ^{230}Th-dated stalagmites in the monsoon region of China shows a consistent long-term increasing trend (Fig. 5), indicating a gradual weakening of the EASM intensity associated with the large-scale weakening of the Asian summer monsoon[28]. However, these $\delta^{18}O_s$ records show differences in long-term trends and amplitude. For example, $\delta^{18}O_s$ records from Wanxiang, Dayu and Dongge caves do not show the long-term increasing trend during last 200 years, and their interdecadal amplitudes are smaller than in other records (Fig. 5). The dating errors of the records from Wanxiang, Dayu, Xiaobailong and Dongge caves are less than 5 years, except for Dongge record.
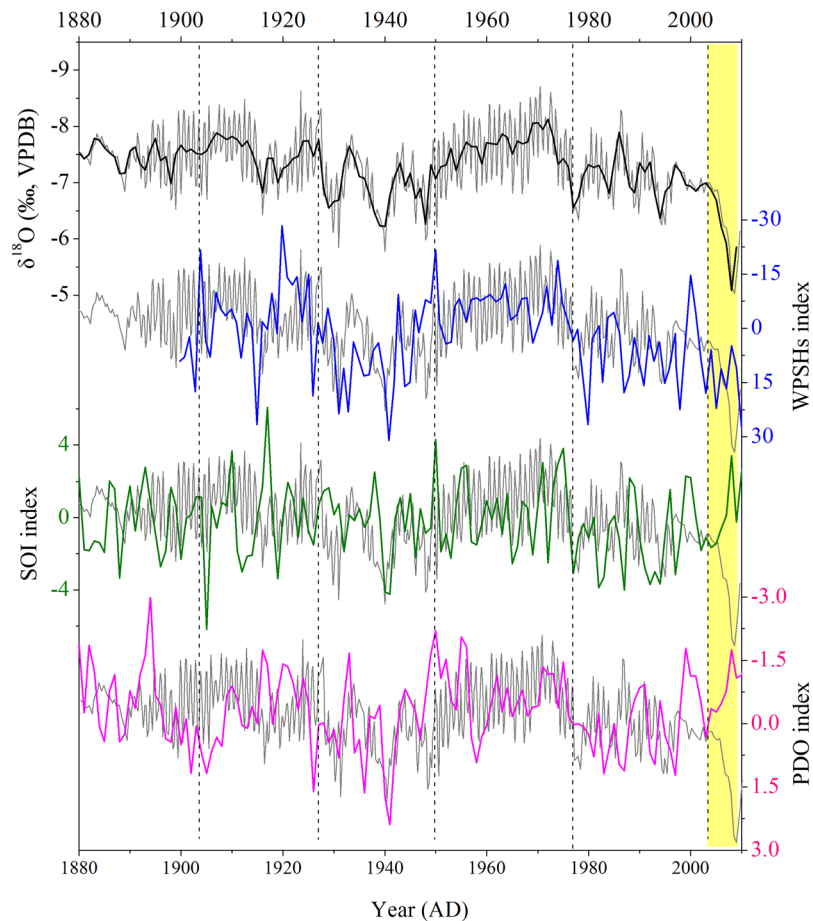
Figure 4. Comparison between annually resolved EM1 $\delta^{18}O$ (black), WPSH$_s$ (blue), SOI (green) and PDO (pink) records during 1880–2009 AD. EM1 $\delta^{18}O$ is positively correlated with the PDO ($r = 0.32$, $p < 0.01$) and negatively correlated with the SOI index ($r = -0.27$, $p < 0.01$) after applying a 5-year average for 1880–2004 AD. The grey lines indicate the original EM1 $\delta^{18}O$ record. The progressively increasing EM1 $\delta^{18}O$ values since 2005 AD (yellow bar) interrupt the coherent correlation with ENSO and PDO. A significantly positive correlation ($r = 0.61$, $p < 0.01$) between $\delta^{18}O$ and WPSH$_s$ is observed after applying a 5-year moving average for 1900–2009 AD.

The records from Shihua, Wuya, Heshang and E'mei caves are based on annual layer counting combined with ^{230}Th dates. Therefore, these differences should not result from the chronology uncertainties. If $\delta^{18}O_s$ is influenced by the "circulation effect", $\delta^{18}O_s$ in SEC, a region more sensitive to circulation changes, should show larger amplitudes. Actually, the long-term $\delta^{18}O_s$ amplitudes of stalagmites from Heshang, Dongge and E'mei caves are smaller than those from Shihua and Wuya caves in North China and Xiaobailong cave in Northwest China (green dotted lines in Fig. 5). In addition, the interdecadal variations are not coherent in these $\delta^{18}O_s$ records from the monsoon region of China, and similarly inconsistent changes are also seen in other studies on decadal-centennial timescales[25,47]. This further demonstrates that $\delta^{18}O_s$ is not only affected by circulation but also by precipitation amount, because the migration of the EASM rainbelt results in different precipitation patterns in the monsoon region of China. Except for the variations in EASM precipitation, changes in NSM precipitation also contribute to the interdecadal divergences seen in the EM1 $\delta^{18}O_s$ record.

What is the relationship between $\delta^{18}O_s$ and seasonal precipitation amount in the study area during different PDO/ENSO phases? On an interannual timescale lower $\delta^{18}O_s$ values are associated with more EASM precipitation during La Niña phases (Figs 2b and 3a) and vice versa. By analyzing the precipitation variability in East China during 14 El Niño events since 1950s Kong and Tu[48] found that less EASM precipitation in May-September in the lower reaches of YRV are associated with El Niño events. Xu et al.[20] showed that the interannual variability in tree-ring cellulose $\delta^{18}O$ data in SEC reveals the variability in May-October precipitation or relative humidity associated with ENSO, with higher (lower) $\delta^{18}O$ values corresponding to less (more) precipitation during El Niño (La Niña) events. Studies based on instrumental and reanalysis data suggest increased spring[5,13] and EAWM precipitation[12,14,15] in SEC associated with El Niño events, indicating increased NSM precipitation during El Niño events on interannual timescales. Therefore, we suggest that the interannual variability recorded by the EM1 $\delta^{18}O_s$ data might also reflect the variability in seasonal precipitation amount, with more (less) EASM and less (more) NSM precipitation during La Niña (El Niño) phases.
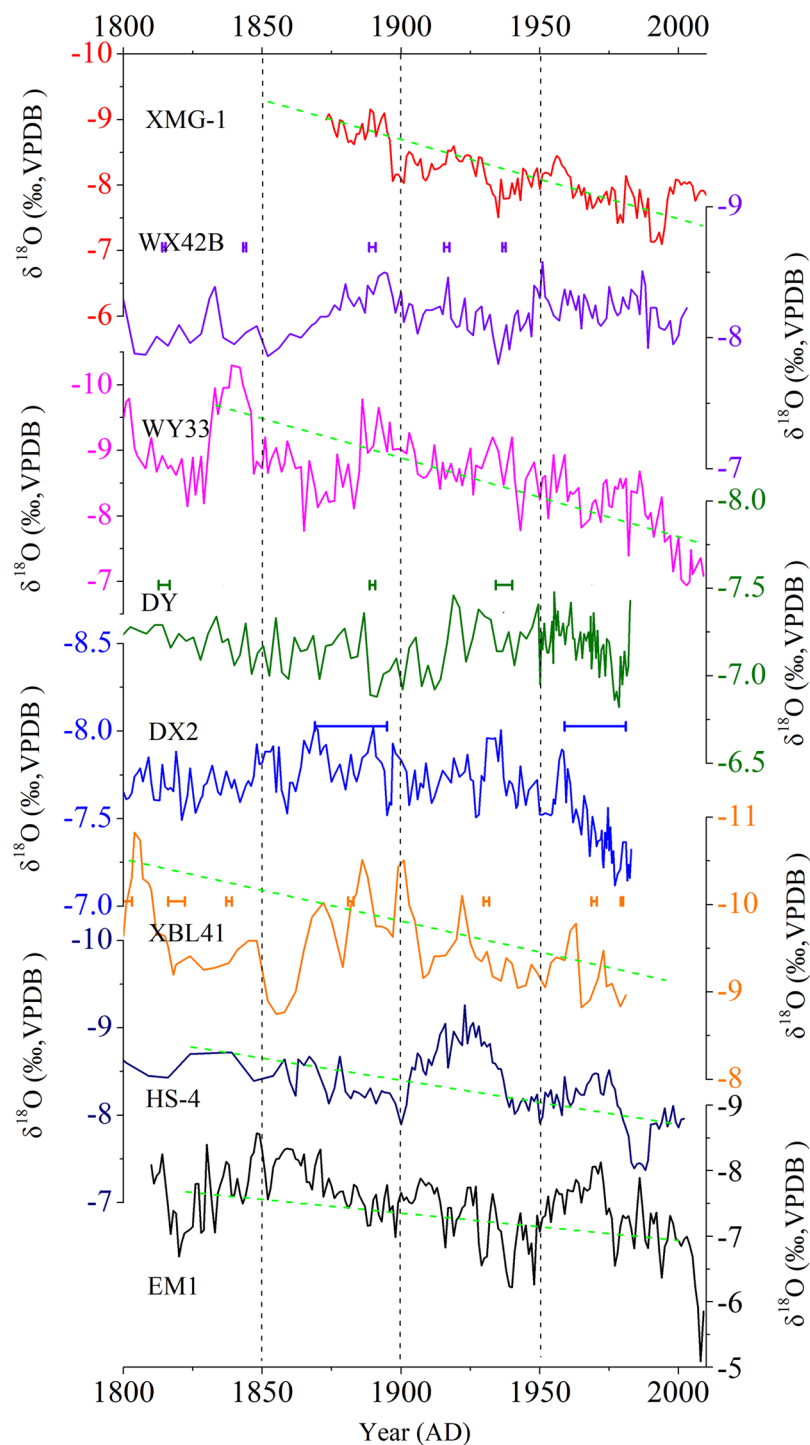
Figure 5. Comparison between high-resolution δ18O records from annually laminated and high-precisely 230Th dated stalagmites in the monsoon region of China: Shihua Cave[28] (red), Wangxiang Cave[27] (purple), Wuya Cave[22] (pink), Heshang Cave[61] (dark blue), Dayu Cave[47] (green), Dongge Cave[38] (blue), Xiaobailong Cave[62] (orange) and E'mei Cave (black, this study). The error bars of the records from Wanxiang, Dayu, Xiaobailong and Dongge caves are also shown. There is no error bar for the other records, because their chronologies are based on the annual layer counting combined with 230Th dates (with larger dating errors).

On interdecadal timescales, many studies demonstrate that more summer monsoon precipitation in June-August in the YRV region results from warm PDO/ENSO phases, and vice versa[7,8,49,50]. These studies indicate that decreased summer rainfall in North China and increased summer rainfall in South China (called "north drought-south flood")[49] result from a strong EASM during cold phases of PDO/ENSO, and vice versa. However, Chan and Zhou[11] found that less (more) early summer monsoon precipitation in May-June in South China results from the warm (cold) phases of PDO/ENSO. This indicates that the pattern of interdecadal variability of June-August precipitation

is opposite to that of May-June precipitation associated with PDO/ENSO. Yang et al.[9] also demonstrated that the effect of the PDO on precipitation anomalies in East China is depends on the month: May-June precipitation patterns in East China are opposite July-August or annual mean patterns. In the study area, the interdecadal variation of precipitation in May also shows an opposite trend to that in June-September for 1951–2009 AD (Supplementary Fig. S8). This further supports our hypothesis that either May-September or June-August precipitation should be used to represent EASM precipitation under different phases of PDO/ENSO (Fig. 3b). Recent observations and simulations indicate that increased (decreased) spring[6] and EAWM[17] precipitation in SEC occurred during warm (cold) phases of ENSO/PDO on interdecadal timescales, indicating more (less) NSM precipitation during warm (cold) phases of ENSO/PDO. This is consistent with our observations (Fig. 3a,b). Therefore, on interdecadal timescales, we suggest that more EASM and less NSM precipitation leading to higher EASM/NSM ratios results in lower $\delta^{18}O_s$ values during the cold phases of ENSO/PDO, and vice versa (Fig. 3b).

The $\delta^{18}O_s$ values gradually increase during the late 20th century reaching a maximum of the entire 200-year record. A similar trend was observed in a tree-ring $\delta^{18}O$ record from Taiwan[36] and a tree-ring $\delta^{13}C$ record from SEC[51]. This trend might be caused by an increased frequency of the central Pacific El Niño (CP El Niño) under continued anthropogenic climate warming during recent decades[36,52]. The anomalous low-level anticyclone and Walker circulation associated with CP El Niño events contributes to anomalously dry conditions over southeastern Asia and an intensified winter monsoon with a deeper East Asian trough at 500 hPa resulting in lower temperatures in South China[53]. CP El Niño events can also lead to decreased spring precipitation in South China and increased spring precipitation in the lower reaches of Yangtze River[13]. More NSM precipitation might also contribute to increased $\delta^{18}O_s$ values. We suggest that the highest $\delta^{18}O_s$ values during the late 20th century result from dry conditions in summer, consistent with the results based on tree-ring $\delta^{13}C$ data from SEC[51]. The synchronously increased $\delta^{13}C$ values in the EM1 and YQ-15 stalagmites (Supplementary Fig. S5) probably indicate degraded vegetation due to these dry conditions[54], further supporting our conclusion.

Methods

^{230}Th dating.   Four subsamples (50–100 mg), drilled using a hand-held carbide dental drill, were analyzed at the Institute of Global Environmental Change, Xi'an Jiaotong University. The chemical procedure used to separate uranium and thorium was similar to that described in Edwards et al.[55]. Uranium and thorium isotopes were measured using a multicollector-inductively coupled plasma-mass spectrometer (MC-ICP-MS). Details about the instrumental setup are explained in Cheng et al.[56].

Stable isotope measurements.   For stable isotope analyses ($\delta^{18}O$ and $\delta^{13}C$), a total of 780 subsamples were micro-milled along the central axis of stalagmite EM1. 370 subsamples were micro-milled at a spatial resolution of 0.1 mm from 0 to 13 mm, and 0.05 mm from 13 to 25 mm distance from the top. These samples were measured using a MAT253 isotope ratio mass spectrometer equipped with a MultiPrep system at Xi'an Jiaotong University. Analytical precision of the $\delta^{18}O$ and $\delta^{13}C$ analyses was better than 0.06‰ and 0.03‰ (1σ), respectively. 410 subsamples were micromilled along the right side of central axis of stalagmite EM1 at a resolution of 0.07 mm from 25 to 53.7 mm distance from the top, and measured on a Thermo Fisher Delta^{plus} XL isotope ratio mass spectrometer linked to a Gasbench II at the University of Innsbruck. Analytical precision was 0.08‰ and 0.06‰ for $\delta^{18}O$ and $\delta^{13}C$, respectively (1σ)[57]. All isotopic values are reported in the δ notation relative to the Vienna Pee Dee Belemnite (VPDB) standards.

Layer counting and $\delta^{18}O$ cycles counting.   On the polished profile of stalagmite EM1, visible laminae consisting of a translucent, dense sub-layer (TDSL) and a white, porous sub-layer (WPSL) can be observed (Supplementary Fig. S1). EM1 was imaged using a confocal laser fluorescent microscope (CLFM) at the State Key Laboratory for Manufacturing Systems Engineering, Xi'an Jiaotong University. The visible WPSL is brightly fluorescent while the visible TDSL is non-fluorescent (Supplementary Fig. S1). We identified 200 ± 3 fluorescent laminae between 0 and 53.6 mm from the top of EM1. The 3-year error is a cumulative error from top to bottom. Because the mean growth rate of EM1 between 0 and 45.6 mm from the top is 0.29 mm/year, we obtained a seasonally-resolved $\delta^{18}O$ record in this section. We counted 159 annual $\delta^{18}O$ cycles between 0 and 45.6 mm from the top of EM1, which is consistent with the layer-counting result using the CLFM.

Data sources.   Monthly instrumental data from the Nanchang and Jiujiang meteorological station during the period 1951–2010 were obtained from the National Climate Center (NCA, http://ncc.cma.gov.cn). Monthly precipitation $\delta^{18}O$ data (1988–1992) from Changsha stations were obtained from the Global Network for Isotopes in Precipitation (GNIP, http://www.iaea.org/). The Southern Oscillation Index (SOI) was obtained from http://www.bom.gov.au/climate/current/soihtm1.shtml. Positive SOI values represent El Niño events and negative values represent La Niña events. The Pacific Decadal Oscillation (PDO) index, defined as the leading standardized principal component of monthly sea-surface temperature (SST) anomalies in the North Pacific Ocean, was taken from http://www.ncdc.noaa.gov/teleconnections/pdo. The west Pacific subtropical high (WPSH) plays an important role in governing the variability over East China. The WPSH strength (WPSH$_s$) index[58] is used to represent the intensity of WPSH, with stronger WPSH$_s$ concurrent with a south-westward extension of WPSH and vice versa.

Spectral analyses.   Were computed using REDFIT software[59] on the PAST platform[60]. The 90% confidence level is shown in Supplementary Fig. S7.

References

1. Wang, B. & Lin, H. Rainy season of the Asian–Pacific summer monsoon. *J. Clim.* **15**, 386–398 (2002).
2. Zong, Y. & Chen, X. The 1998 flood on the Yangtze, China. *Natural Hazards* **22**, 165–184 (2000).
3. Tian, S.-F. & Yasunari, T. Climatological aspects and mechanism of spring persistent rains over central China. *J. Meteorol. Soc. Japan. Ser. II* **76**, 57–71 (1998).

4. Wan, R. & Wu, G. Temporal and spatial distributions of the spring persistent rains over Southeastern China. *J. Meteorol. Res.* **23**, 598–608 (2009).
5. Wan, R., Zhao B. K. & Hou, Y. L. Interannual variability of spring persistent rain over southeastern China and its effect factor. *Plateau Meteorol.* **27**, 118–123 (In Chinese with English abstract) (2008).
6. Wu, X. & Mao, J. Interdecadal modulation of ENSO-related spring rainfall over South China by the Pacific Decadal Oscillation. *Clim. Dyn.* **47**, 3203–3220 (2016).
7. Yu, L., Furevik, T., Otterå, O. H. & Gao, Y. Modulation of the Pacific Decadal Oscillation on the summer precipitation over East China: a comparison of observations to 600-years control run of Bergen Climate Model. *Clim. Dyn.* **44**, 475–494 (2015).
8. Dong, X. & Xue, F. Phase transition of the Pacific decadal oscillation and decadal variation of the East Asian summer monsoon in the 20th century. *Adv. Atm. Sci.* **33**, 330–338 (2016).
9. Yang, Q., Ma, Z. & Xu, B. Modulation of monthly precipitation patterns over East China by the Pacific Decadal Oscillation. *Clim. Change*, https://doi.org/10.1007/s10584-016-1662-9 (2016).
10. Yang, F. & Lau, K. M. Trend and variability of China precipitation in spring and summer: linkage to sea-surface temperatures. *Intern. J. Clim.* **24**, 1625–1644 (2004).
11. Chan, J. C. & Zhou, W. PDO, ENSO and the early summer monsoon rainfall over south China. *Geophys. Res. Lett.* **32**, L08810, https://doi.org/10.1029/2004GL022015 (2005).
12. Zhou, L. T. & Wu, R. Respective impacts of the East Asian winter monsoon and ENSO on winter rainfall in China. *J. Geophys. Res.* **115**, D02107, https://doi.org/10.1029/2009JD012502 (2010).
13. Feng, J. & Li, J. Influence of El Niño Modoki on spring rainfall over south China. *J. Geophys. Res.* **116**, D13102, https://doi.org/10.1029/2010JD015160 (2011).
14. Zhou, L. T. Impact of East Asian winter monsoon on rainfall over southeastern China and its dynamical process. *Int. J. Clim.* **31**, 677–686 (2011).
15. Zhang, L., Fraedrich, K., Zhu, X., Sielmann, F. & Zhi, X. Interannual variability of winter precipitation in Southeast China. *Theor. Appl. Clim.* **119**, 229–238 (2015).
16. Wang, S., Huang, J., He, Y. & Guan, Y. Combined effects of the Pacific decadal oscillation and El Nino-southern oscillation on global land dry–wet changes. *Sci. Rep.* **4**, 6651 (2014).
17. Kim, J.-W., Yeh, S.-W. & Chang, E.-C. Combined effect of El Niño-Southern Oscillation and Pacific Decadal Oscillation on the East Asian winter monsoon. *Clim. Dyn.* **42**, 957–971, https://doi.org/10.1007/s00382-013-1730-z (2014).
18. Xu, C. *et al.* Inter-and intra-annual tree-ring cellulose oxygen isotope variability in response to precipitation in Southeast China. *Trees* **30**, 785–794 (2016).
19. Xu, C., Zheng, H., Nakatsuka, T. & Sano, M. Oxygen isotope signatures preserved in tree ring cellulose as a proxy for April–September precipitation in Fujian, the subtropical region of southeast China. *J. Geophys. Res.* **118**, 12,805–812,815, https://doi.org/10.1002/2013JD019803 (2013).
20. Xu, C. *et al.* Potential utility of tree ring δ18O series for reconstructing precipitation records from the lower reaches of the Yangtze River, southeast China. *J. Geophys. Res.* **121**, 3954–3968, https://doi.org/10.1002/2015JD023610 (2016).
21. Tan, M. *et al.* Applications of stalagmite laminae to paleoclimate reconstructions: comparison with dendrochronology/climatology. *Quat. Sci. Rev.* **25**, 2103–2117 (2006).
22. Tan, L. *et al.* Cyclic precipitation variation on the western Loess Plateau of China during the past four centuries. *Sci. Rep.* **4**, 6381, https://doi.org/10.1038/srep06381 (2014).
23. Orland, I. J. *et al.* Seasonal resolution of Eastern Mediterranean climate change since 34ka from a Soreq Cave speleothem. *Geochim. Cosmochim. Acta* **89**, 240–255 (2012).
24. Dorale, J. A., Edwards, R. L., Ito, E. & Gonzalez, L. A. Climate and vegetation history of the midcontinent from 75 to 25 ka: a speleothem record from Crevice Cave, Missouri, USA. *Science* **282**, 1871–1874 (1998).
25. Cai, Y. *et al.* The variation of summer monsoon precipitation in central China since the last deglaciation. *Earth Planet. Sci. Lett.* **291**, 21–31 (2010).
26. Hendy, C. H. The isotopic geochemistry of speleothems—I. The calculation of the effects of different modes of formation on the isotopic composition of speleothems and their applicability as palaeoclimatic indicators. *Geochim. Cosmochim. Acta* **35**, 801–824 (1971).
27. Zhang, P. *et al.* A test of climate, sun, and culture relationships from an 1810-year Chinese cave record. *Science* **322**, 940–942, https://doi.org/10.1126/science.1163965 (2008).
28. Li, X. *et al.* The East Asian summer monsoon variability over the last 145 years inferred from the Shihua Cave record, North China. *Sci. Rep.* **7**, 7078, https://doi.org/10.1038/s41598-017-07251-3 (2017).
29. Dayem, K. E., Molnar, P., Battisti, D. S. & Roe, G. H. Lessons learned from oxygen isotopes in modern precipitation applied to interpretation of speleothem records of paleoclimate from eastern Asia. *Earth Planet. Sci. Lett.* **295**, 219–230 (2010).
30. Tan, M. Circulation effect: response of precipitation δ18O to the ENSO cycle in monsoon regions of China. *Clim. Dyn.* **42**, 1067–1077 (2014).
31. Tan, M. Circulation background of climate patterns in the past millennium: Uncertainty analysis and re-reconstruction of ENSO-like state. *Sci. Chi. Earth Sci.* **59**, 1225–1241 (2016).
32. Baker, A. J. *et al.* Seasonality of westerly moisture transport in the East Asian summer monsoon and its implications for interpreting precipitation δ18O. *J. Geophys. Res.* **120**, 5850–5862 (2015).
33. Cai, Z., Tian, L. & Bowen, G. J. ENSO variability reflected in precipitation oxygen isotopes across the Asian Summer Monsoon region. *Earth Planet. Sci. Lett.* **475**, 25–33 (2017).
34. Cheng, H. *et al.* The Asian monsoon over the past 640,000 years and ice age terminations. *Nature* **534**, 640–646 (2016).
35. Yang, H., Johnson, K., Griffiths, M. & Yoshimura, K. Interannual controls on oxygen isotope variability in Asian monsoon precipitation and implications for paleoclimate reconstructions. *J. Geophys. Res.* **121**, 8410–8428 (2016).
36. Liu, Y. *et al.* Recent enhancement of central Pacific El Nino variability relative to last eight centuries. *Nature Commun.* **8**, 15386, https://doi.org/10.1038/ncomms15386 (2017).
37. Jiang, X. Y., Li, Z. Z., Li, J. Q., Kong, X. G. & Guo, Y. Stalagmite δ18O record from Yuhua Cave over the past 500 years and its regional climate significance. *Sci. Geogr. Sin.* **32**, 207–212 (In Chinese with English abstract) (2012).
38. Zhao, K. *et al.* A high-resolved record of the Asian Summer Monsoon from Dongge Cave, China for the past 1200 years. *Quat. Sci. Rev.* **122**, 250–257 (2015).
39. Zhang, D. The method for reconstruction of climate series for the last 500 years and its reliability. Collected Papers of Meteorological Science and Technology (4), edited by: Central Meteorological Bureau, Meteorological Press, Beijing, China, 17–26 (In Chinese) (1983).
40. Huang, R., Chen, J., Wang, L. & Lin, Z. Characteristics, processes, and causes of the spatio-temporal variabilities of the East Asian monsoon system. *Adv. Atmos. Sci.* **29**, 910–942 (2012).
41. Zhou, W. & Chan, J. C. ENSO and the South China Sea summer monsoon onset. *Int. J. Climatol.* **27**, 157–167 (2007).
42. Liu, J. *et al.* Asian summer monsoon precipitation recorded by stalagmite oxygen isotopic composition in the western Loess Plateau during AD 1875–2003 and its linkage with ocean-atmosphere system. *Chin. Sci. Bull.* **53**, 2041–2049 (2008).
43. Jing, Y. Y., Li, S., Wan, J.-H. & Luo, F.-F. Relationships between the oxygen isotopes in East Asian stalagmites and large-scale atmospheric and oceanic modes. *Atmos. Ocean. Sci. Lett.* **7**, 540–545 (2014).

44. Zhao, M. *et al.* Changes in climate and vegetation of central Guizhou in southwest China since the last glacial reflected by stalagmite records from Yelang Cave. *J. Asian Earth Sci.* **114**, 549–561 (2015).
45. Li, H. C. *et al.* The first high-resolution stalagmite record from Taiwan: Climate and environmental changes during the past 1300 years. *J. Asian Earth Sci.* **114**, 574–587 (2015).
46. Zhang, Y., Tian, Q., Guillet, S. & Stoffel, M. 500-yr. precipitation variability in Southern Taihang Mountains, China, and its linkages to ENSO and PDO. *Clim. Change*, https://doi.org/10.1007/s10584-016-1695-0 (2016).
47. Tan, L., Cai, Y., Cheng, H., An, Z. & Edwards, R. L. Summer monsoon precipitation variations in central China over the past 750 years derived from a high-resolution absolute-dated stalagmite. *Palaeogeogr. Palaeoclimatol. Palaeoecol.* **280**, 432–439 (2009).
48. Kong, C. Y. & Tu, Q. P. Influence of El Niño events on summer precipitation in east China under different climatic backgrounds. *J. Nanjing Inst. Meteorol.* **1**, 84–88 (In Chinese with English abstract) (2003).
49. Gong, D. Y. & Ho, C. H. Shift in the summer rainfall over the Yangtze River valley in the late 1970s. *Geophys. Res. Lett.* **29**, 1436, https://doi.org/10.1029/2001GL014523 (2002).
50. Zhou, T. *et al.* Why the western Pacific subtropical high has extended westward since the late 1970s. *J. Clim.* **22**, 2199–2215 (2009).
51. Liu, Y. *et al.* Tree-ring stable carbon isotope-based April–June relative humidity reconstruction since ad 1648 in Mt. Tianmu, China. *Clim. Dyn*, https://doi.org/10.1007/s00382-017-3718-6 (2017).
52. Yeh, S. W. *et al.* El Niño in a changing climate. *Nature* **461**, 511 (2009).
53. Yuan, Y. & Yang, S. Impacts of different types of El Niño on the East Asian climate: focus on ENSO cycles. *J. Clim.* **25**, 7702–7722 (2012).
54. Zhang, H. *et al.* Large variations of $\delta^{13}C$ values in stalagmites from southeastern China during historical times: implications for anthropogenic deforestation. *Boreas* **44**, 511–525 (2015).
55. Edwards, R. L., Chen, J. & Wasserburg, G. ^{238}U-^{234}U-^{230}Th-^{232}Th systematics and the precise measurement of time over the past 500,000 years. *Earth Planet. Sci. Lett.* **81**, 175–192 (1987).
56. Cheng, H. *et al.* Improvements in ^{230}Th dating, ^{230}Th and ^{234}U half-life values, and U–Th isotopic measurements by multi-collector inductively coupled plasma mass spectrometry. *Earth Planet. Sci. Lett.* **371**, 82–91 (2013).
57. Spötl, C. Long-term performance of the Gasbench isotope ratio mass spectrometry system for the stable isotope analysis of carbonate microsamples. *Rapid Commun. Mass Spectrome.* **25**, 1683–1685 (2011).
58. Mu, Q. Z., Wang, S. W., Zhu, J. H. & Gong, D. Variations of the western Pacific subtropical high in summer during the last hundred years. *Chin. J. Atmos. Sci.* **25**, 787–797 (2001).
59. Schulz, M. & Mudelsee, M. REDFIT: estimating red-noise spectra directly from unevenly spaced paleoclimatic time series. *Comput. Geosci.* **28**, 421–426 (2002).
60. Hammer, Ø., Harper, D. & Ryan, P. Paleontological statistics software: Package for education and data analysis. *Palaeontol. Electron.* **4**, 9 (2001).
61. Hu, C. *et al.* Quantification of Holocene Asian monsoon rainfall from spatially separated cave records. *Earth Planet. Sci. Lett.* **266**, 221–232 (2008).
62. Tan, L. *et al.* Decreasing monsoon precipitation in southwest China during the last 240 years associated with the warming of tropical ocean. *Clim. Dyn.* **48**, 1769–1778 (2017).
63. Yatagai, A. *et al.* A 44-year daily gridded precipitation dataset for Asia based on a dense network of rain gauges. *Sola* **5**, 137–140 (2009).

Acknowledgements

Author Contributions

H.W.Z. and H.C. conceived the project; H.W.Z. wrote the first draft of the paper. H.C., C.S., Y.J.C. and A.S. contributed to the manuscript revision at different stages. H.W.Z., C.S. and Y.F.N. contributed to ^{230}Th dating and isotope measurements. L.C.T. and H.Y. provided the suggestion for interpreting the stalagmite record. H.W.Z., Y.L., X.L.L. and G.K. did the correlation and time series analyses. F.Z. and J.Y.Z. helped make the thin-section and the analysis of CLFM. All authors discussed the results, edited and commented on the final manuscript.

Additional Information

Supplementary information accompanies this paper at https://doi.org/10.1038/s41598-018-30112-6.

Competing Interests: The authors declare no competing interests.

Publisher's note: Springer Nature remains neutral with regard to jurisdictional claims in published maps and institutional affiliations.